Juntao Fu, Jing Xu, Jing Lin, Jürgen Köhler and Shuiquan Deng*

"Flat/steep band model" for superconductors containing Bi square nets

https://doi.org/10.1515/znb-2019-0191
Received November 8, 2019; accepted November 29, 2019

Abstract: The crystal structures of a new family of superconductors containing a Bi square net and their electronic structures around the Fermi level have been reviewed. The structures of these compounds can be viewed as stacked layers denoted by [Bi][(*RE*)(M_2Bi$_2$)(*RE*)] *RE* = rare earth or alkaline earth metal, *M* = transition metal. Flat/steep band features are shown to exist in all these new superconductors, though the pairing mechanisms may be very different. The Dirac Fermion behavior is reviewed and its implications are discussed.

Keywords: bismuth; crystal structure; electronic structure; square nets; superconductivity.

Dedicated to: Professor Arndt Simon on the Occasion of his 80th birthday.

1 General overview

Since its discovery in mercury [1], superconductivity has remained at the frontiers of condensed matter physics and material science. Because of the zero-electric resistance property and the Meissner effect below the critical transition temperature, T_C, superconductors have been used to produce superconducting magnets for high and stable magnetic field applications. Such magnets have been widely used in various applications, e.g. magnetic resonance imaging (MRI) nuclear magnetic resonance (NMR), mass spectrometers, SQUIDS, etc., including large scientific devices, e.g. the Large Hadron Collider (LHC) in CERN and the superconducting Tokamak "Eastern Super Ring" (East) in Hefei. Maglev trains, smart grids, and quantum computing may be further future applications [2–4].

On the other hand, the attempt to understand the origin of superconductivity has never come to an end because new exotic superconductors continue to be discovered. Among the proposed models or theories, the Ginzburg–Landau theory [5] is the most successful phenomenological model which provided a heuristic explanation for the macroscopic properties of superconductors. In particular, it predicted the 2e charges for a superconducting charge carrier and the type-I and type-II classification for the superconductors according to their behavior in a magnetic field [6]. The microscopic understanding for conventional superconductivity was accomplished with the establishment of the BCS theory [7]. This theory explained the superconducting state as a phase coherent condensate of Cooper pairs which are formed due to second-order electron-phonon interactions. The BCS theory provided explanations for the isotope effect, the Meissner effect and the characteristic electronic specific heat, etc. and could be reduced to the Ginzburg–Landau theory when the temperature is close to T_C as shown by Gor'kov [8]. The BCS theory encountered serious difficulties when organic, heavy-fermion, high-T_C cuprates, and the magnesium boride superconductorswere discovered [9]. The appearance of iron-pnictide(Pn)-based superconductors [10], and the superconductivity of H_2S (T_C = 80 K) at ~160 GPa [11] as well as that of the LaH_{10} (T_C = 250 K) at ~170 GPa [12] challenged further the basis of the conventional theories. To understand these exotic superconductivities, a few theories or models have been developed along the lines as described in Ref. [9]. Though none of these theories has so far been unanimously accepted, some radical ones such as anyon superconductivity [13] have gradually been abandoned due to the lack of experimental supports. A growing consensus on a correct theory is that it should consider at least (1) the pairing of charge carriers; (2) the pairing mechanism mediated by bosons beyond phonons

***Corresponding author: Shuiquan Deng,** State Key Laboratory of Structural Chemistry, Fujian Institute of Research on the Structure of Matter, Chinese Academy of Sciences, Fuzhou, Fujian 350002, P.R. China, e-mail: sdeng@fjirsm.ac.cn
Juntao Fu and Jing Xu: State Key Laboratory of Structural Chemistry, Fujian Institute of Research on the Structure of Matter, Chinese Academy of Sciences, Fuzhou, Fujian 350002, P.R. China; and University of Chinese Academy of Sciences, Beijing 100049, P.R. China
Jing Lin: State Key Laboratory of Structural Chemistry, Fujian Institute of Research on the Structure of Matter, Chinese Academy of Sciences, Fuzhou, Fujian 350002, P.R. China
Jürgen Köhler: State Key Laboratory of Structural Chemistry, Fujian Institute of Research on the Structure of Matter, Chinese Academy of Sciences, Fuzhou, Fujian 350002, P.R. China; and Max Planck Institute for Solid State Research, Heisenbergstrasse 1, 70569 Stuttgart, Germany

such as the spin excitation, etc. (3) the multiband electronic structures around the Fermi level. The most challenging problem is that simple physical models lack the capacity to include many important degrees of freedom such as spin, orbital, dynamics, defects as well as chemical complexity [9, 14], whose quantitative knowledges are also beyond the capability of cutting-edge first-principle methods.

An evident disadvantage of the physical models is that the relevance of chemical bonding to superconductivity was completely ignored, though early on Bilz et al. drew attention to the "dynamic covalency" [15]. In 1997, Simon proposed a hypothesis, calling for a simultaneous presence of flat and steep band portions at the Fermi level as a necessary condition for a metal to become a superconductor [16]. Later on, a flat/steep band model as a normal state character of superconductors was developed based on the chemical pairwise interactions [9, 17–21].

$$H_e = \Sigma_k \varepsilon_k^s s_k^+ s_k + \Sigma_k \varepsilon_k^f f_k^+ f_k \quad (1)$$

where ε_k^s and ε_k^f in eq. (1) represent the energy dispersions in the steep and flat band, respectively [20, 21]. These two kinds of electrons interact with phonons in a very different way [20, 21], and thus naturally lead to a two-band superconductivity mechanism [22] for conventional superconductors. The inter-band pairing which is important for enhancing T_C was shown to be due to the breakdown of the Born-Oppenheimer approximation by Whangbo et al. [23]. Recently, Deng et al. have shown that the generalized coherent state constructed by pure group theory can be used to describe the superconducting state. Within this framework the flat band feature in the normal state can be explained as a residue of the pairwise interaction between the charge carriers [24]. After the proposal of the flat/steep band model, it was tested by using many superconductors with phonon glued Cooper pairs [9, 25–27], and the results corroborated the model. Though the model has also been checked with high-T_C cuprates [9] and iron-based [28] superconductors; it needs to be scrutinized more with further superconductors of exotic nature.

The recently discovered new family of superconductors [29–34] containing Bi square nets, though having relatively low T_C, are very interesting because it may be based on topological superconductivity [35]. In this work, we provide a survey with a focus on the electronic structures around the Fermi level. In cases where the electronic structures are not available from the literature, we have calculated them by using the first-principles method implemented in the VASP [36, 37] code.

2 Method of calculations

The calculations for $CeNi_{0.8}Bi_2$ were performed by using the Vienna ab initio simulation package (VASP) [36, 37] based on the density functional theory (DFT) [38, 39] and the generalized gradient approximation (GGA) of Perdew–Burke–Ernzerhof (PBE) [40] for the exchange-correlation functional. The LSDA + U method [41] was used to treat the strongly correlated 4*f* and 3*d* electrons. The values of the parameter *U* and the exchange integral *J* for the 4*f* electrons of the Ce ions are chosen as 8 and 1 eV, while those for the 3*d* electrons of the Ni ions are chosen as 4 and 1 eV, respectively [42, 43]. In this work, the basis sets for Ce, Ni and Bi are $4f^1 5s^2 5p^6 5d^1 6s^2$, $3d^8 4s^2$ and $5d^{10} 6s^2 6p^3$, respectively. The convergence tolerance of the total energy was set at 1×10^{-5} eV, and that of the maximum force in geometry optimization at 0.001 eV $Å^{-1}$. The Monkhorst-Pack scheme for a *k*-points grid $6 \times 6 \times 3$ was used, and the plane wave basis set energy cutoff was set at 400 eV. The tetrahedron method with Blöchl corrections was utilized in the integrations.

3 Electronic structure features around the Fermi level

So far, superconducting phases containing Bi square nets in their structures have been found in only four types of compounds [29–34]. It is well-known that the Bi square net has a strong spin-orbit coupling effect due to the relativistic effect, which is a favorable condition to realize the time-reversal breaking topological superconductivity and to search for the Majorana fermions [35]. It is thus also crucial to find the location of the Bi-*p* states in the actual electronic band structure for their relevance to the possible topological superconductivity.

3.1 RE_2O_2Bi (*RE* = La–Er, or Y)

The crystal structure of RE_2O_2Bi belongs to the tetragonal $ThCr_2Si_2$ structure type, in which the Bi^{2-} anions form a square net sandwiched between $(RE_2O_2)^{2+}$ cations made up of edge-sharing ORE_4 tetrahedra (Fig. 1) [44–46]. In 2011, Mizoguchi and Hosono systematically studied the electric transport properties of the RE_2O_2Bi compounds and found that a metal-insulator transition can be induced by changing the size of the rare earth ions *RE*, an effect of chemical pressure [47]. Because of the well-known

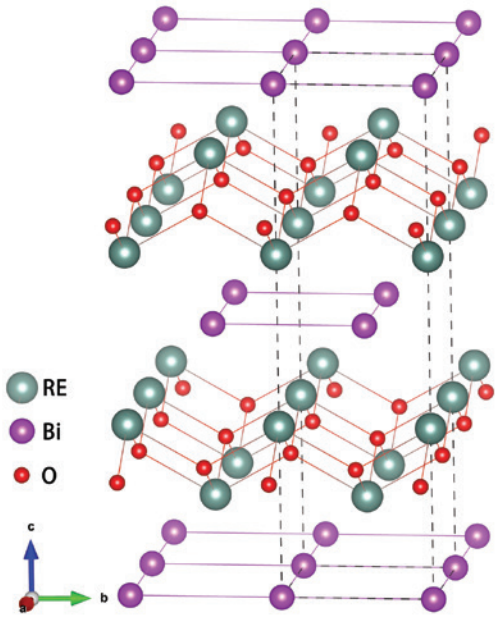

Fig. 1: The crystal structure of RE_2O_2Bi shown with a $2\times2\times1$ supercell, the figure is drawn by using the data of Y_2O_2Bi. (*RE* = La–Er, or Y).

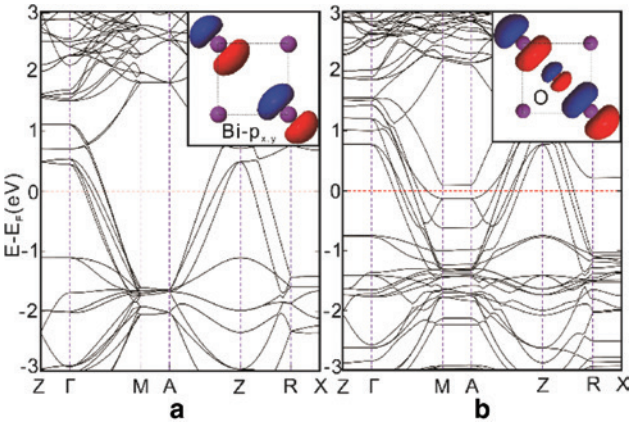

Fig. 2: Band structures of Y_2O_2Bi (left) and $Y_2O_{2.125}Bi$ (right) calculated using a (2*a*, 2*b*, c) supercell. Γ = (0, 0, 0), X = (0.5, 0, 0), *M* = (0.5, 0.5, 0), Z = (0, 0, 0.5), R = (0, 0.5, 0.5), A = (0.5, 0.5, 0.5). The inset shows why a flat band far below the Fermi level is pushed up to the Fermi level from the undoped case (a) to the oxygen-doped case (b) [50].

lanthanide contraction, the radius of the rare earth elements decreases from La^{3+} to Er^{3+} and accordingly the Bi–Bi distance in the Bi square net of the corresponding compounds RE_2O_2Bi decreases from 4.08 to 3.85 Å. It was found that the metallic behavior becomes more prominent with the size decrease of the rare earth ion RE^{3+}, however, no superconducting transition was detected down to 1.8 K [47]. The formal charge of a pnicogen (Pn) was considered important for the stability of its square nets against the Peierls distortions by Tremel and Hoffmann [46]. Recently, the 2D electronic transport property characteristic of the strong spin-orbital coupling in a Bi^{2-} square net was revealed with experiments on Y_2O_2Bi thin films [48]. Kim et al. further analyzed the importance of the spin-orbital coupling of the Bi-6*p* electrons in suppressing the charge density wave (CDW) instability of the Bi square nets in the structures of RE_2O_2Bi compounds [49].

Superconducting transitions at T ~2 K were observed in the oxygen doped Y_2O_2Bi samples by Sei et al. [33]. The nominal superconducting phase range of $Y_2O_{2+x}Bi$, within which the T_C does not change much (ΔT_C ~0.19), is $0 \le x \le 0.67$. Because of the tiny amount of the doping, the locations of the O atoms are not determined by experiment, though it is suggested that they are located nearby the $(Y_2O_2)^{2+}$ layer [33]. By using the first-principles method, our group [50] found that the energetically most favorable location for the additional O atoms are the centers of the Bi squares. Our calculations have indicated that the parent Y_2O_2Bi phase has a metallic conductivity (Fig. 2a) without the presence of flat bands around the Fermi level. With the additional O atoms introduced into the Bi square nets, a surprising effect occurs, namely the flat bands far below the Fermi level are pushed up to the Fermi level due to the antibonding interaction between the O-2*p* orbitals and the Bi-6*p* orbitals (Fig. 2b), creating a flat/steep band condition for superconductivity. According to our results, both the metallicity and the superconductivity are confined in the 2D Bi square nets which are sandwiched by the insulating $(Y_2O_2)^{2+}$ layers. The topological properties of the current system is worth further studies because Majorana fermions have been predicted to exist at the interface of a superconductor and a topological insulator [51].

According to a recent report [34], a partially oxidized "Er_2O_2Bi", a new superconducting phase, was prepared by sintering Er, Er_2O_3 together with CaO. If the actual composition of the sample is close to Er_2O_2Bi, one may expect that a similar situation as in Y_2O_2Bi occurs, though the crystal and electronic structure of the superconducting phase is not yet known.

3.2 *REM*Bi_2 (*RE* = rare earth or IIA metals; *M* = transition metals)

Compounds with the chemical formula *REM*Bi_2, *RE* = rare earth or alkaline earth metal and *M* = transition metal, crystallize in the tetragonal $ZrCuSi_2$-type structure. As shown in Fig. 3, the structure of these compounds can be readily described by [Bi][(*RE*)(M_2Bi_2)(*RE*)] comparable

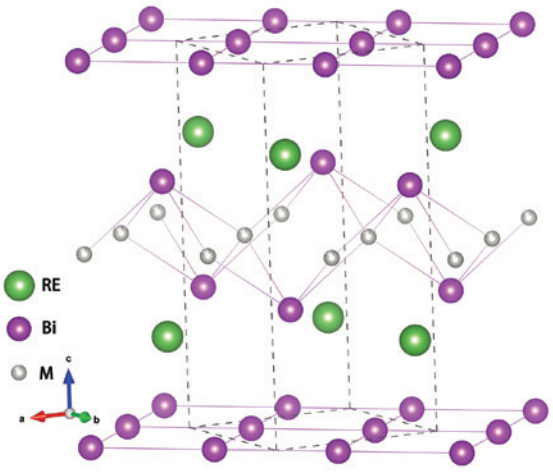

Fig. 3: The crystal structure of $ZrCuSi_2$-type *REM*Bi_2 compounds, (*RE* = rare earth or alkaline earth metal; *M* = transition metal). The figure is drawn with the crystallographic data of $LaPd_{0.85}Bi_2$.

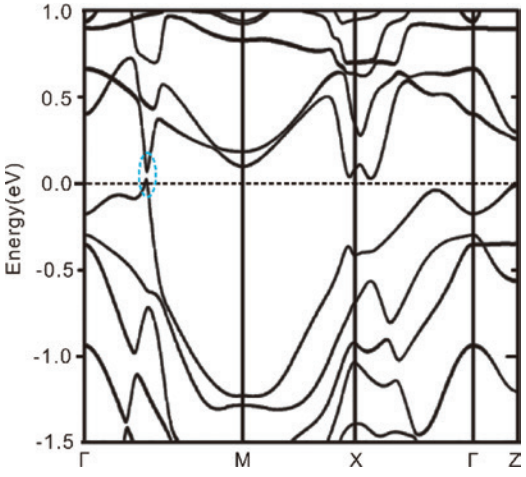

Fig. 4: Band structure of cAFM-$SrMnBi_2$ with a Dirac point around the Fermi level indicated in a dotted blue circle. The spin-orbital coupling is considered in the calculations [53].

to [Bi][Y_2O_2] of Y_2O_2Bi, with alternating layers of square nets of Bi [Bi], the rare earth layers (RE) and (M_2Bi_2) core layers. The core layer has the PbO-type structure as the FeAs layers in the Fe-based superconductors [30]. The distance between the rare earth layer and the core layer is in general very small (~0.9 Å in $CeNiBi_2$), however, the *RE*–Bi distance can be large (e.g. 3.33~3.45 Å in $CeNiBi_2$). The metric details may change with the size and formal charge of the rare earth elements *RE* and those of the transition elements *M*, however, the bonding feature of the structure is the same. The function of the embedded layers of rare earth or alkaline earth atoms can be understood in terms of a charge reservoir to donate electrons into the adjacent layers [52], thus shifting the Fermi level outside of the band region of the Bi square nets. Consequently, the Bi–Bi bond lengths in the Bi square nets are shortened from ~3.87 Å in Y_2O_2Bi to ~3.2 Å in the *REM*Bi_2 compounds and any physical phenomena may be affected by this.

3.2.1 *REM*Bi_2 (*RE* = alkaline earth metal; *M* = transition metal)

$SrMnBi_2$ is an interesting representative of the *REM*Bi_2 family, for *RE* = IIA (alkaline earth) metals [53], in which a strong anisotropic Dirac point has been identified [54], and thus a new platform for studying Dirac Fermions was suggested. In Fig. 4 the calculated band structure based on a Néel-ordering ground state at the GGA + SOC level is shown. It is evident that a Dirac point occurs along the Γ–M line, which results from the Bi-6$p_{x,y}$ orbitals of the Bi square net. Based on this band structure it is hard to explain the observed Fermi surface and the metallicity, because bands crossing the Fermi level are absent. The band gap was considered as resulting from the spin-orbital coupling by Park et al. [54]. In a subsequent study more Dirac points around the Fermi level have been found, and a checkerboard antiferromagnetic ground state (cAFM) has been detected by using GGA + spin polarized calculations [55]. This study [55] provides a more reasonable explanation for the observed metallicity and the Fermi surface [54], at least qualitatively. However, the discrepancies of these two studies have not been resolved to date. On one hand, the latter work did not consider the spin-orbital coupling, on the other hand, none of them considered the strong correlation effect of the Mn-3*d* electrons, which was found to be important by the authors of Ref. [55]. As can be clearly seen from Fig. 4 or fig. 8 in Ref. [55], the flat/steep band condition is not satisfied for the ground state of $SrMnBi_2$. In fact, it is a cAFM state instead of a superconducting one below T ~290 K [54, 55].

It was predicted that doping the Mn-3*d* band away from the half-filled condition may suppress the magnetic order and lead to superconductivity [55]. An interesting fact is that the calculated band structure (Fig. 5) for the paramagnetic phase (PM) of $SrMnBi_2$ evidently meets the flat/band condition [55]. However, it has remained unclear whether the superconductivity observed for a $SrMnBi_2$ + Bi sample at T ~5.7 K [32] is related to the PM phase. The flat bands shown in Fig. 5 are mainly of Mn-3*d* character, while the steep bands are mainly of the Bi-6$p_{x,y}$ character, which implies very heterogenous Fermi surface

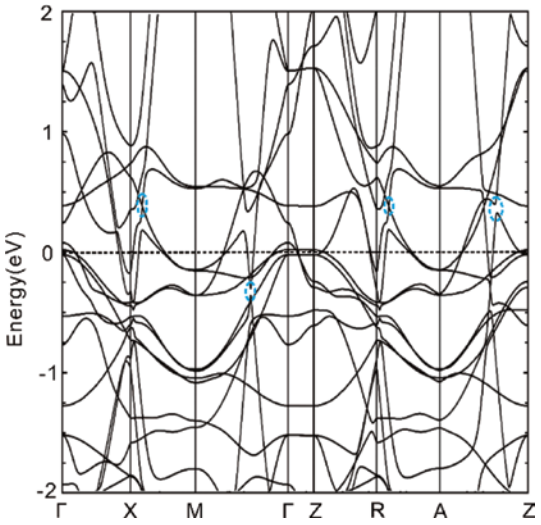

Fig. 5: Band structure of PM-$SrMnBi_2$ showing the flat/steep band feature around the Fermi level. A few Dirac-like points around the Fermi level are indicated in dotted blue circles [54].

pieces and new coupling between them. Dirac electron behavior and possible topological superconductivity in this system is an issue worth of further investigations. Originally, this superconductivity was explained as an interface superconductivity between $SrMnBi_2$ and Bi [32]. A precise theoretical description of the doping effect on the $SrMnBi_2$ system is still lacking.

Anisotropic Dirac fermion behavior was also observed in the $BaMnBi_2$ structure [56, 57] which has a cAFM ground state at low temperature too. The calculations carried out early indicated that the Bi-6*p* and Mn-3*d* hybridization is significant. This compound has a superconducting transition at ~3.4 K under ~2.6 GPA [58], an effect of physical doping. An explanation for the superconductivity is not available, because the variations of the electronic structure under high pressure are not yet known.

3.2.2 *RE*$PdBi_2$ (*RE* = La, Ce, Nd)

Superconducting transitions at T_C ~2.1 K were observed in the $LaPd_{1-x}Bi_2$ phase, $0.2 \le x \le 0.45$, and within this range the transition temperature remains almost unchanged [30]. A similar transition at T_C ~3.2 K was also observed in $NdPd_{0.77}Bi_2$ [59]. The normal oxidation state of the lanthanoid ions is +3, which means that they can donate one more electron than the alkaline earth (IIA) metal atoms, e.g. Sr in $SrMnBi_2$, to the adjacent layers, i.e. the core (Pd_2Bi_2) layers or the [Bi] layers of Bi square nets. Considering the non-stoichiometry, the Bi-6$p_{x,y}$ bands of the Bi square net may have a fractional filling as discussed by Papoian and Hoffmann [60] for similar compounds. As mentioned in the last paragraphs, the ground state of the *REM*Bi_2 family has in general a magnetic order which is absent in the $LaPd_{1-x}Bi_2$ phases. It was argued by Han et al. [30] that the vacancies on the Pd sites have a pronounced influence on the Fermi surface to suppress the putative CDW. However, whether the absence of the magnetic ordering is also due to the vacancy scattering at the Pd sites has not been mentioned. As shown in Fig. 6, the feature that the steep bands cross the Fermi level is not lacking, while the zero group velocity states are also present around the Fermi level. The latter band feature has been defined as "flat band" states in our earlier work [17]. In fact, even if one shifts the Fermi level down, due to the Pd vacancies, it may also meet such states nearby R and Z points and those along the X–A line in the first Brillouin zone (BZ). As shown in Fig. 6, the Pd-4*d* orbitals dominate the contributions at the Fermi level, while the contributions of Bi and La in the (La_2Bi_2) core layer and of the Bi square nets are smaller and nearly the same between each other. The scattering role of the vacant defects at the Pd sites was emphasized by Han et al. to infer a single-band and s-wave superconductivity. However, it must be pointed out that in Han et al.'s calculations a rigid-band approximation was assumed, without considering

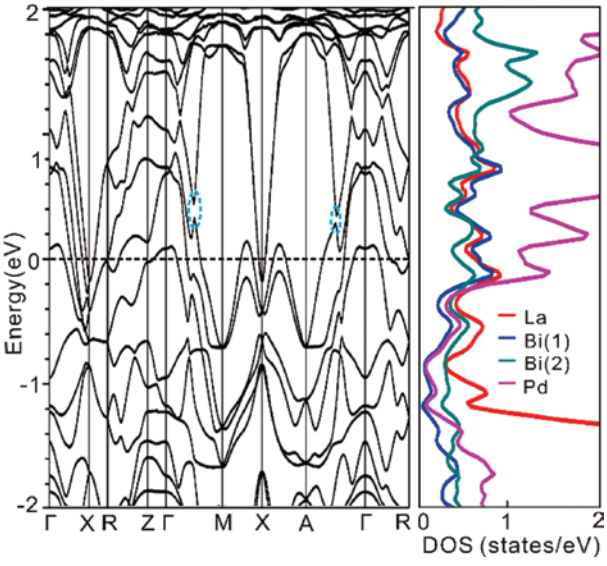

Fig. 6: The band structure of stoichiometric $LaPdBi_2$ near the Fermi level. The flat band shows up as a small portion of a band with vanishing group velocity. A few Dirac-like points around the Fermi level are indicated in blue dotted circles. In the right panel, Bi(1) denotes Bi atoms in the core layer (Pd_2Bi_2), and Bi(2) denotes Bi atoms on the Bi square net [30].

the actual vacancy structure of the $LaPd_{1-x}Bi_2$ phase. The question, how the electronic structure changes when vacancies are introduced, has yet remained an elusive issue. The ground state of $CePd_{1-x}Bi_2$ was characterized as AFM below 6 K by Han et al. [30].

3.2.3 *RE*Ni_xBi_2, (*RE* = La, Ce, Nd, Gd, Tb, Dy, and Y)

Mizoguchi et al. described the structure of $CeNi_{0.8}Bi_2$ as alternate stacking of $[CeNixBi]^{\delta+}$ and $Bi^{\delta-}$ layers, which is equivalent to our universal description, [Bi][(Ce)($Ni_{2x}Bi_2$)(Ce)]. A Bi square net also occurs in $CeNi_{1-x}Sb_{1+y}Bi_{1-y}$ phases [61]. The original reports [29] on the superconducting transition at 4.2 K based on a polycrystalline $CeNi_xBi_2$ sample was questioned by another measurement on single crystal samples [62]. Superconductivity was observed in a single crystal sample of $LaNi_xBi_2$ only, while for *RE*Ni_xBi_2 (*RE* = Ce–Nd, Sm, Gd–Dy) local moment like behavior and AFM ground states were observed at low temperature. Kodama et al. [63] used a neutron powder diffraction method to study the magnetic structure of $CeNi_{0.8}Bi_2$ and suggested the coexistence of the AFM order and superconductivity. So far, this controversy has not been resolved, though the single crystal data may be more convincing. Nevertheless, the two studies based on powder samples have suggested that the superconductivity is due to the light electrons from the Bi square nets, while heavy electrons from the Ce-4*f* states are responsible for the AFM order. To understand the physical properties of $CeNi_{0.8}Bi_2$, we calculated the band structure of $CeNi_{0.8}Bi_2$ with the spin-polarized LSDA + U method (see computational details).

Our calculations indicate that the flat bands along the Γ–Z direction consist of ~80% Ce-*f* orbital (Fig. 7). The steep bands along the X–Γ direction are composed of ~50–67% Ce-4*f* plus 40–26% Bi-6*p*, respectively. For the other steep bands, the Ce-4*f* orbital contributes even more than for those along the X–Γ direction. Our calculations indicate that the electronic structure around the Fermi level is dominated by the Ce-4*f* contributions. However, the steep bands around the Fermi level is a result of the hybridization between Bi-4*p* and Ce-4*f* orbitals. This hybridization provides mobility to the heavy fermions on the Ce-4*f* bands. Regardless of the superconductivity mechanism, the flat/steep band feature is present in the calculated band structure. Our calculations do not support the explanation of independent Bi-6*p* and Ce-4*f* states. Magnetic moments are not found at any atomic sites, which can be compatible with the absence of any weak AFM order [29].

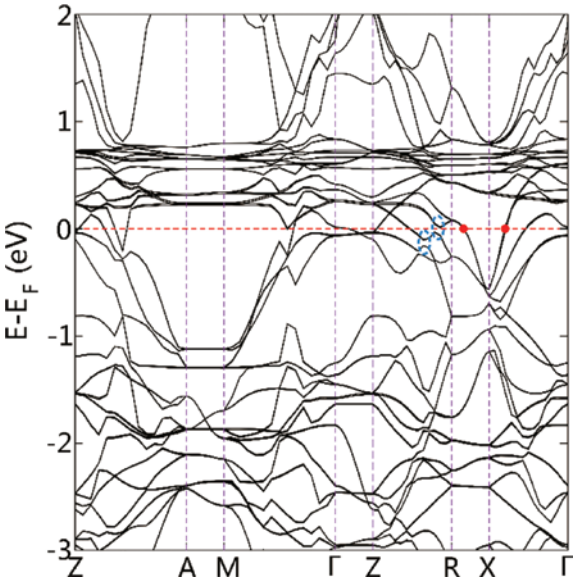

Fig. 7: Band structures of $CeNiBi_2$ showing the presence of flat/steep feature around the Fermi level. A few Dirac points around the Fermi level are indicated in the blue dotted circle. Red dots indicate the steep bands we analyzed.

The latter possibility was not investigated in this work; however, it will be part of future studies.

4 Summary and perspective

The crystal and electronic structures of a new family of superconductors containing Bi square nets have been reviewed with focus on their universal features. The structures of these compounds can be viewed as stacked layers denoted as [Bi][(*RE*)(M_2Bi_2)(*RE*)], where the alkaline or rare earth layers (*RE*) can be removed as in the Y_2O_2Bi structure and vacancies are present in the core layers ($M_{2x}Bi_2$). In fact, the Bi atoms can also be replaced by other pnictogen elements. The flat/steep band feature appears in all the reviewed superconductors, though the actual pairing mechanism may be unknown. For Y_2O_2Bi, both the flat and steep bands are dominantly of Bi-6$p_{x,y}$ character. In $LaPd_{1-x}Bi_2$, the flat bands consist of Pd-4*d* orbitals, while the steep bands have mainly Bi-6$p_{x,y}$ character. In $CeNi_xBi_2$, the flat bands stem from Ce-4*f* orbitals, while the steep band originates from a hybrid of Ce-4*f* and Bi-6$p_{x,y}$ orbitals. A Dirac fermion behavior is more prominent in $SrMnBi_2$ and $LaPd_{1-x}Bi_2$, while in Y_2O_2Bi and $CeNi_xBi_2$ this character is not visible or less prominent due to the smearing effect of the strong spin-orbital coupling and correlation effects. Due to the vacancies a rugged energy

landscape is created in the systems, however, their influence has not been well studied. The interaction between the Bi square nets and the core (M_2Pn_2) layers is worth to be further studied with the inclusion of strong correlation and spin-orbital coupling.

Acknowledgements: This work is financially supported by the National Natural Science Foundation (NSF) of China (61874122, 21703251); the NSF of Fujian Province (2019J01121, 2019J05151); the Strategic Priority Research Program of the Chinese Academy of Sciences (CAS) (XDB20000000); the National Key Research and Development Program of China (2016YFB0701001); Youth Innovation Promotion of CAS (2019302); 100 talents program of CAS and Fujian Province.

References

[1] H. K. Onnes, *Leiden Comm.* **1911**, *119b*, 122–124.
[2] A. Twin, J. Brown, F. Domptail, R. Bateman, R. Harrison, M. Lakrimi, Z. Melhem, P. Noonan, M. Field, S. Hong, K. Marken, H. Miao, J. Parrell, Y. Zhang, *IEEE Trans. Appl. Supercond.* **2007**, *17*, 2295–2298.
[3] J. Linder, J. Robinson, *Nat. Phys.* **2015**, *11*, 307–315.
[4] H. Thomas, A. Marian, A. Chervyakov, S. Stückrad, D. Salmieri, C. Rubbia, *Renew. Sustain. Energy Rev.* **2016**, *55*, 59–72.
[5] V. L. Ginzburg, L. D. Landau, *Sov. Phys. JETP* **1950**, *20*, 1064–1082.
[6] A. A. Abrikosov, *Sov. Phys. JETP* **1957**, *5*, 1174–1182.
[7] J. Bardeen, L. N. Cooper, J. R. Schrieffer, *Phys. Rev.* **1957**, *108*, 1175–1204.
[8] L. P. Gor'kov, *Sov. Phys. JETP* **1960**, *37*, 593–599.
[9] S. Deng, A. Simon, J. Köhler, *Struct. Bond.* **2005**, *114*, 1348–1351.
[10] H. Takahashi, K. Igawa, K. Arii, Y. Kamihara, M. Hirano, H. Hosono, *Nature* **2008**, *453*, 376–378.
[11] Y. Li, J. Hao, H. Liu, Y. Li, Y. Ma, *J. Chem. Phys.* **2014**, *140*, 174712.
[12] A. P. Drozdov, P. P. Kong, V. S. Minkov, S. P. Besedin, M. A. Kuzovnikov, S. Mozaffari, L. Balicas, F. F. Balakirev, D. E. Graf, V. B. Prakapenka, E. Greenberg, D. A. Knyazev, M. Tkacz, M. I. Eremets, *Nature* **2019**, *569*, 528–531.
[13] V. Kalmeyer, R. B. Laughlin, *Phys. Rev. Lett.* **1987**, *59*, 2095.
[14] M. Sigrist, K. Ueda, *Rev. Mod. Phys.* **1991**, *63*, 239–312.
[15] J. Hafner, W. Hanke, H. Biltz in *Electron-Phonon Interactions and Phase Transitions*, (Ed.: T. Riste), Plenum Press, New York, London, **1977**, p. 200.
[16] A. Simon, *Angew. Chem., Int. Ed. Engl.* **1997**, *36*, 1788–1806. (CAS journal abbreviation before 1998).
[17] S. Deng, A. Simon, J. Köhler, *Angew. Chem. Int. Ed.* **1998**, *37*, 640–643. (CAS journal abbreviation after 1998).
[18] S. Deng, A. Simon, J. Köhler, *J. Am. Chem. Soc.* **2002**, *124*, 10712–10717.
[19] S. Deng, A. Simon, J. Köhler, *J. Supercond.* **2004**, *17*, 227–231.
[20] S. Deng, A. Simon, J. Köhler, *Int. J. Mod. Phys. B* **2005**, *19*, 29–36.
[21] S. Deng, A. Simon, J. Köhler, *Int. J. Mod. Phys. B* **2007**, *21*, 3082–3085.
[22] H. Suhl, B. T. Matthias, L. R. Walker, *Phys. Rev. Lett.* **1959**, *3*, 552–554.
[23] M.-H. Whangbo, S. Deng, J. Köhler, A. Simon, *ChemPhysChem* **2018**, *19*, 3191–3195.
[24] S. Deng, C. Felser, J. Köhler, *J. Mod. Phys.* **2013**, *4*, 10–13.
[25] S. Deng, J. Köhler, A. Simon, *Angew. Chem. Int. Ed.* **2006**, *45*, 599–602.
[26] S. Deng, A. Simon, J. Köhler in *High Tc Superconductors and Related Transition Metal Oxides*, (Eds.: A. Bussmann-Holder, H. Keller), Springer-Verlag, Berlin, **2007**, pp. 201–211.
[27] S. Deng, A. Simon, J. Köhler, *Angew. Chem. Int. Ed.* **2008**, *47*, 6703–6706.
[28] S. Deng, J. Köhler, A. Simon, *Phys. Rev. B* **2009**, *80*, 214508.
[29] H. Mizoguchi, S. Matsuishi, M. Hirano, M. Tachibana, E. Takayama-Muromachi, H. Kawaji, H. Hosono, *Phys. Rev. Lett.* **2011**, *106*, 057002.
[30] F. Han, C. D. Malliakas, C. C. Stoumpos, M. Sturza, H. Claus, D. Y. Chung, M. G. Kanatzidis, *Phys. Rev. B* **2013**, *88*, 144511.
[31] T. Yajima, K. Nakano, F. Takeiri, Y. Nozaki, Y. Kobayashi, H. Kageyama, *J. Phys. Soc. Jpn.* **2013**, *82*, 033705.
[32] K. Vinod, A. Bharathi, A. T. Satya, S. Sharma, T. R. Devidas, A. Mani, A. K. Sinha, S. K. Deb, V. Sridharan, C. S. Sundar, *Solid State Commun.* **2014**, *192*, 60–63.
[33] R. Sei, S. Kitani, T. Fukumura, H. Kawaji, T. Hasegawa, *J. Am. Chem. Soc.* **2016**, *138*, 11085–11088.
[34] K. Terakado, R. Sei, H. Kawasoko, T. Koretsune, D. Oka, T. Hasegawa, T. Fukumura, *Inorg. Chem.* **2018**, *57*, 10587–10590.
[35] X.-L. Qi, S.-C. Zhang, *Rev. Mod. Phys.* **2010**, *83*, 175–179.
[36] G. Kresse, J. Furthmüller, *Comp. Mater. Sci.* **1996**, *6*, 15–50.
[37] G. Kresse, J. Furthmüller, *Phys. Rev. B* **1996**, *54*, 11169.
[38] P. Hohenberg, W. Kohn, *Phys. Rev.* **1964**, *136*, B864–B871.
[39] W. Kohn, L. J. Sham, *Phys. Rev.* **1965**, *140*, A1133–A1138.
[40] J. P. Perdew, K. Burke, M. J. Ernzerhof, *Phys. Rev. Lett.* **1996**, *77*, 3865–3868.
[41] G. Kresse, M. Marsman, J. Furthmüller, *VASP the Guide*, University of Vienna, Vienna (Austria) **2016**.
[42] J. Rusz, P. M. Oppeneer, N. J. Curro, R. R. Urbano, B.-L. Young, S. Lebègue, P. G. Pagliuso, L. D. Pham, E. D. Bauer, J. L. Sarrao, Z. Fisk, *Phys. Rev. B* **2008**, *77*, 245124.
[43] J. Kaczkowski, M. Pugaczowa-Michalska, A. Jezierski, *Acta. Phys. Pol. A* **2018**, *133*, 408–410.
[44] W. Jeitschko, B. Jaberg, *J. Solid State Chem.* **1980**, *35*, 312–317.
[45] E. Brechtel, G. Cordier, H. Schäfer, *J. Less-Common Met.* **1981**, *79*, 131–138.
[46] W. Tremel, R. Hoffmann, *J. Am. Chem. Soc.* **1987**, *109*, 124–140.
[47] H. Mizoguchi, H. Hosono, *J. Am. Chem. Soc.* **2011**, *133*, 2394–2397.
[48] R. Sei, T. Fukumura, T. Hasegawa, *ACS Appl. Mater. Interfaces* **2015**, *7*, 24998–25001.
[49] H. Kim, C.-J. Kang, K. Kim, J. H. Shim, B. I. Min, *Phys. Rev. B* **2016**, *93*, 125116.
[50] X. Y. Cheng, E. E. Gordon, M. H. Whangbo, S. Q. Deng, *Angew. Chem. Int. Ed.* **2017**, *56*, 10123–10126.
[51] L. Fu, C. L. Kane, *Phys. Rev. Lett.* **2008**, *100*, 096407.
[52] L. Wang, X. Ma, Q.-K. Xue, *Supercond. Sci. Technol.* **2016**, *29*, 123001.
[53] G. Cordier, H. Schäfer, *Z. Naturforsch.* **1977**, *32b*, 383–386.

[54] J. Park, G. Lee, F. Wolff-Fabris, Y. Y. Koh, M. J. Eom, Y. K. Kim, M. A. Farhan, Y. J. Jo, C. Kim, J. H. Shim, J. S. Kim, *Phys. Rev. Lett.* **2011**, *107*, 126402.
[55] J. K. K. Wang, L. L. Zhao, Q. Yin, G. Kotliar, M. S. Kim, M. C. Aronson, E. Morosan, *Phys. Rev. B* **2011**, *84*, 064428.
[56] L. Li, K. Wang, D. Graf, L. Wang, A. Wang, C. Petrovic, *Phys. Rev. B* **2016**, *93*, 115141.
[57] H. Ryu, S. Y. Park, L. Li, W. Ren, J. B. Neaton, C. Petrovic, C. Hwang, S.-K. Mo, *Sci Rep.* **2018**, *8*, 15322.
[58] H. Chen, L. Li, Q. Zhu, J. Yang, B. Chen, Q. Mao, J. Du, H. Wang, M. Fang, *Sci. Rep.* **2017**, *7*, 1634.
[59] F. M. Zhang, W. Zhou, C. Q. Xu, S. W. Liu, J. Y. Zhang, M. Xia, X. Xu, B. Qian, *J. Alloys Compd.* **2019**, *782*, 170–175.
[60] G. A. Papoian, R. Hoffmann, *Angew. Chem. Int. Ed.* **2000**, *39*, 2408–2448.
[61] K. Schäfer, B. Gerke, O. Niehaus, R. Pöttgen, *Z. Naturforsch.* **2014**, *69b*, 409–416.
[62] X. Lin, W. E. Straszheim, S. L. Bud’ko, P. C. Canfield, *J. Alloys Compd.* **2013**, *554*, 304–311.
[63] K. Kodama, S. Wakimoto, N. Igawa, S. Shamoto, H. Mizoguchi, H. Hosono, *Phys. Rev. B* **2011**, *83*, 214512.